Journal of Inorganic Biochemistry 200 (2019) 110811

Contents lists available at ScienceDirect

Journal of Inorganic Biochemistry

journal homepage: www.elsevier.com/locate/jinorgbio

Antiproliferative activity of heterometallic sodium and potassium-dioxidovanadium(V) polymers

Manas Sutradhar[a,*], Elisabete C.B.A. Alegria[a,b], Francesco Ferretti[a], Luís R. Raposo[c], M. Fátima C. Guedes da Silva[a], Pedro V. Baptista[c], Alexandra R. Fernandes[a,c,*], Armando J.L. Pombeiro[a]

[a] Centro de Química Estrutural, Instituto Superior Técnico, Universidade de Lisboa, Av. Rovisco Pais, 1049-001 Lisboa, Portugal
[b] Chemical Engineering Department, Instituto Superior de Engenharia de Lisboa, Instituto Politécnico de Lisboa, R. Conselheiro Emídio Navarro, 1, 1959-007 Lisboa, Portugal
[c] UCIBIO, Departamento Ciências da Vida, Faculdade de Ciências e Tecnologia, Universidade Nova de Lisboa, Campus Caparica, 2829-516 Caparica, Portugal

ARTICLE INFO

Dedicated to Prof. Debbie C. Crans as a recognition of her distinguished contributions for the advancement of Inorganic and Bioinorganic Chemistries.

Keywords:
Dioxidovanadium(*V*)
Aroylhydrazone
X-ray structure
Antiproliferative agent

ABSTRACT

The syntheses of the heterometallic sodium and potassium-dioxidovanadium 2D polymers, $[NaVO_2(1\kappa NOO';2\kappa O''\text{-L})(H_2O)]_n$ **(1)** and $[KVO_2(1\kappa NOO';2\kappa O';3\kappa O''\text{-L})(EtOH)]_n$ **(2)** (where the κ notation indicates the coordinating atoms of the polydentate ligand L) derived from (3,5-di-*tert*-butyl-2-hydroxybenzylidene)-2-hydroxybenzohydrazide (H_2L) are reported. The polymers were characterized by IR, NMR, elemental analysis and single crystal X-ray diffraction analysis. The antiproliferative potential of **1** and **2** was examined towards four human cancer cell lines (ovarian carcinoma, A2780, colorectal carcinoma, HCT116, prostate carcinoma, PC3 and breast adenocarcinoma, MCF-7cell lines) and normal human fibroblasts. Complex **1** and **2** showed the highest cytotoxic activity against A2780 cell line (IC_{50} 8.2 and 11.3 μM, respectively) with **1** > **2** and an IC_{50} in the same range as cisplatin (IC_{50} 3.4 μM; obtained in the same experimental conditions) but, interestingly, with no cytotoxicity to healthy human fibroblasts for concentrations up to 75 μM. This high cytotoxicity of **1** in ovarian cancer cells and its low cytotoxicity in healthy cells demonstrates its potential for further biological studies. Our results suggest that both complexes induce ovarian carcinoma cell death via apoptosis and autophagy, but autophagy is the main biological cause of the reduction of viability observed and that ROS (reactive oxygen species) may play an important role in triggering cell death.

1. Introduction

The development of bioactive metal complexes is a promising approach in biological and pharmacological studies. Among the various transition metal complexes, oxidovanadium(IV and V) complexes have achieved a considerable interest in drug discovery and some of them exhibit insulin-mimetic activity, anti-microbial activity, tumor growth inhibition and prophylaxis against carcinogenesis [1–11]. They also play important roles as reducers of hyperlipidemia, hypertension and obesity, and enhancers of oxygen affinity by hemoglobin and myoglobin [1–18]. To date, only a few oxidovanadium(IV) compounds, such as bis(maltolato)oxidovanadium(IV) (BMOV) and bis(ethylmaltolato) oxidovanadium(IV) (BEOV), have been tested in clinical trials [19].

The antiproliferative activity of vanadium complexes [10,20–23] disclosed by successful in vitro studies over the past few decades have promoted anticancer research into the preclinical stage, e.g., for breast cancer, liver cancer, colorectal cancer and leukemia [24].

The understanding of the molecular effects of vanadium complexes in cancer cells has been a matter of concern and, in this regard, cytotoxicity, apoptosis induction and biological targets such as DNA and proteins have been investigated [10,24–26]. The modes of action have also been demonstrated for most cytostatic vanadium compounds although some of them, for example vanadocenes, may directly intercalate with DNA [3,7,10].

Aroylhydrazones are a type of pro-ligand that plays an important role to stabilize oxidovanadium(IV and V) complexes [24–33], displaying also good biological activities when complexed with different metals [10,34–36]. Indeed, Ni(II) and Co(II) complexes of an asymmetrical aroylhydrazone displayed moderate cytotoxic effects against human hepatocellular carcinoma (SMMC-7721) and human lung adenocarcinoma (A549) cell lines, that might be correlated with DNA

* Corresponding authors.
E-mail addresses: manas@tecnico.ulisboa.pt (M. Sutradhar), ma.fernandes@fct.unl.pt (A.R. Fernandes).

https://doi.org/10.1016/j.jinorgbio.2019.110811
Received 27 May 2019; Received in revised form 22 August 2019; Accepted 25 August 2019
Available online 27 August 2019
0162-0134/

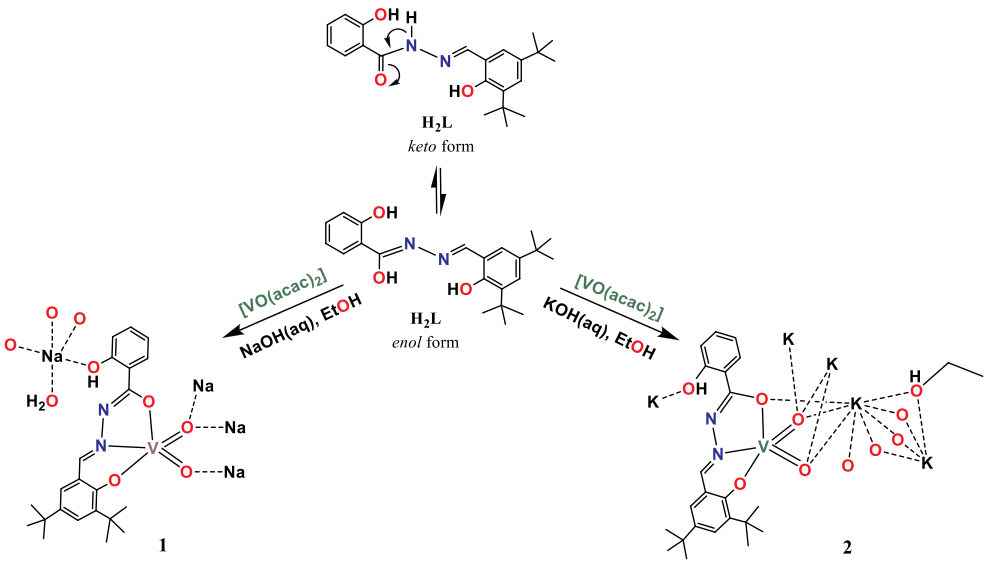

Scheme 1. Synthesis of **1** and **2**.

interaction [35]. Recently, four mixed ligand aroylhydrazone and N-donor heterocyclic Lewis base Cu(II) complexes [CuL(X)]$_2$ [L refers to the dianionic form of (5-bromo-2-hydroxybenzylidene)-2-hydroxybenzohydrazide; X = pyrazine (Pz; **1**), pyridine (Py; **2**), imidazole (Imz; **3**) and 3-pyridinecarbonitrile (3-PyCN; **4**)] were synthesized, with complex **4** exhibiting a high cytotoxic activity against ovarian (A2780) and colorectal (HCT116) carcinoma cells, with IC_{50} much lower than those for human healthy fibroblasts [34]. The cytotoxic effect of complex **4** in HCT116 cells was attributed by the authors to a cell death mechanism via apoptosis and not via autophagy [34]. In this work the authors showed that the Schiff base pro-ligand 5-bromo-2-hydroxybenzylidene)-2-hydroxybenzohydrazide had no antiproliferative effect in the tested cell lines and that the antiproliferative potential of complex **4** was due to complexation with Cu(II) in the presence of the secondary ligand, N-donor heterocyclic Lewis base, 3-pyridinecarbonitrile [34]. Indeed, the other secondary ligands used in that work did not induce any proliferative effect in those tumor cell lines, showing the importance of ligands selection for the cytotoxic effect [34]. Recently, a series of mononuclear metal complexes of Co(III), Ni(II) and Cu(II) with 2-(2,4-dichlorobenzamido)-N′-(3,5-di-tert-butyl-2- hydroxybenzylidene) benzohydrazide have been synthesized with significant anti-inflammatory and antioxidant potential [36], however in vitro cytotoxicity was not evaluated.

In this study, we report the syntheses and characterization of two heterometallic sodium and potassium-dioxidovanadium 2D polymers, [$NaVO_2$(1κN*OO'*;2κ*O"*-L)(H_2O)]$_n$ **(1)** and [KVO_2(1κN*OO'*;2κ*O'*;3κ*O"*-L)(EtOH)]$_n$ **(2)** (where the κ notation indicates the coordinating atoms of the polydentate ligand L, as suggested by IUPAC) derived from (3,5-di-*tert*-butyl-2-hydroxybenzylidene)-2-hydroxybenzohydrazide (H_2L) aroylhydrazone. The stability in biological media and the antiproliferative potential of the two complexes were examined towards four different human cancer cell lines. Their direct cytotoxicity against normal human fibroblasts was also assessed.

2. Experimental

2.1. General materials and procedures

All synthetic work was performed in air. The reagents and solvents were obtained from commercial sources and used as received, i.e., without further purification or drying. [VO(acac)$_2$] (acac = acetylacetonate) was used as the metal source for the synthesis of **1** and **2**. C, H, and N elemental analyses were carried out on a Perkin Elmer PE 2400 Series II by the Microanalytical Service of the Instituto Superior Técnico. Infrared spectra (4000–400 cm^{-1}) were recorded on a BRUKER VERTEX 70 or Jasco FT/IR-430 instrument in KBr pellets, wavenumbers are in cm^{-1}. Mass spectra were run in a Varian 500-MS LC Ion Trap Mass Spectrometer equipped with an electrospray (ESI) ion source. For electrospray ionization, the drying gas and flow rate were optimized according to the particular sample with 35 p.s.i. nebulizer pressure. Scanning was performed from *m/z* 100 to 1200 in methanol solution. The compounds were observed in the negative mode (capillary voltage = 80–105 *V*). The ^{1}H NMR spectra were recorded at room temperature on a Bruker Avance II + 300 (UltraShield™ Magnet) spectrometer operating at 300.130 MHz for proton. The chemical shifts are reported in ppm using tetramethylsilane as the internal reference. ^{51}V NMR spectra were recorded on a Bruker 400 UltraShield spectrometer at ambient temperature (297 K) in DMSO–d_6. The vanadium chemical shifts are quoted relative to external [$VOCl_3$]. UV spectra were recorded in an Evolution 300 UV–Vis spectrophotometer (Thermo Scientific).

2.2. Synthetic procedures

2.2.1. Synthesis of the pro-ligand H_2L

The pro-ligand (3,5-di-*tert*-butyl-2-hydroxybenzylidene)-2-hydroxybenzohydrazide (H_2L) was prepared according to literature [37] by condensation of the corresponding salicylhydrazide with 3,5-di-*tert*-butyl-2-hydroxybenzaldehyde.

2.2.2. Syntheses of the dioxidovanadium(V) complexes

Polymers [$NaVO_2$(1κN*OO'*;2κ*O"*-L)(H_2O)]$_n$ (**1**) and [KVO_2(1κN*OO'*;2κ*O'*;3κ*O"*-L)(EtOH)]$_n$ (**2**) were synthesized by using a common general method (Scheme 1) given below.

To a 30 mL ethanolic suspension of H_2L (0.368 g, 1.00 mmol), 0.265 g (1.00 mmol) of [VO(acac)$_2$] was added and the reaction mixture refluxed. After 1 h the mixture was cooled down to room temperature and an aqueous solution of 0.1 M NaOH (for **1**) or 0.1 M KOH (for **2**) was added with constant stirring until a pH of ca. 9 was obtained. The reflux was taken up for another hour. The resultant dark yellow solution was filtered, and the filtrate was kept in air. After ca. 3 d, X-ray quality yellow crystals were isolated, washed 3 times with cold ethanol and dried in open air.

[$NaVO_2$(1κN*OO'*;2κ*O"*-L)(H_2O)]$_n$ (**1**) – Yield 76%. Anal. Calcd for $C_{22}H_{28}N_2NaO_6V$: C, 53.88; H, 5.76; N, 5.71. Found: C, 53.84; H, 5.73; N, 5.68. IR (KBr; cm^{-1}): 2954 ν(OH), 1602 ν(C=N), 1251 ν(C–O)

enolic, 1087 ν(N—N), 956, 902 ν(V=O). ESI-MS(−): *m/z* 448 $[VO_2(L)]^-$ (100%). ^{1}H NMR (DMSO-d_6, δ): 11.64 (s, 1H,OH), 9.01 (s, 1H, –CH=N), 7.85–6.80 (m, 6H, C_6H_4), 1.39 (s, 9H, CH_3), 1.30 (s, 9H, CH_3). ^{51}V NMR (DMSO-d_6, δ) - 538.

$[KVO_2(1\kappa NOO';2\kappa O';3\kappa O''\text{-L})(EtOH)]_n$ (**2**) – Yield 73%. Anal. Calcd for $C_{24}H_{32}N_2KO_6V$: C, 53.92; H, 6.03; N, 5.24. Found: C, 53.89; H, 6.01; N, 5.21. IR (KBr; cm^{-1}): 2947 ν(OH), 1600 ν(C=N), 1258 ν(C—O) enolic, 1085 ν(N—N), 953, 914 ν(V=O). ESI-MS(−): *m/z* 448 $[VO_2(L)]^-$ (100%). ^{1}H NMR (DMSO-d_6, δ): 12.31 (s, 1H,OH), 9.04 (s, 1H, –CH=N), 7.84–6.91 (m, 6H, C_6H_4), 1.35 (s, 9H, CH_3), 1.29 (s, 9H, CH_3) 5.38 (q, 4H, CH_2, *J* = 7.01 OC_2H_5), 1.68 (t, 6H, CH_3, *J* = 6.97, OC_2H_5). ^{51}V NMR (DMSO-d_6, δ) - 542.

2.3. X-ray measurements

X-ray single crystals of **1** and **2** were immersed in cryo-oil mounted in Nylon loops and measured at a temperature of 296 (**1**) or 180 K (**2**). Intensity data were collected using a Bruker AXS-KAPPA APEX II or a Bruker APEX-II PHOTON 100 with graphite monochromated Mo-Kα (λ 0.71073) radiation. Data were collected using 0.5° per frame and a full sphere of data was obtained. Cell parameters were retrieved using Bruker SMART [37] software and refined using Bruker SAINT [38] on all the observed reflections. Absorption corrections were applied using SADABS [38]. Structures were solved by direct methods by using the SHELXS package [39] and refined with SHELXL–2018/3 [39]. Calculations were performed using the WinGX System-Version 2014.1 [40]. The hydrogen atoms of hydroxide groups were found in the difference Fourier map and those of water (in **2**) were inserted in calculation; the isotropic thermal parameters were set at 1.5 times the average thermal parameters of the belonging oxygen atoms. Coordinates of hydrogen atoms bonded to carbon atoms were included in the refinement using the riding-model approximation with the Uiso(H) defined as 1.2Ueq of the parent aromatic atoms. The methyl groups of the C19-containing *tert*-butyl moiety in **1**, and the ethyl group of the ethanol ligand in **2** were disordered between two positions and were modelled by means of the PART instruction in SHELXL. Crystal data and refinement parameters are presented in Table S1 and selected bond distances and angles are given in the legends of Figs. 1 and 2. Crystallographic data for the structural analysis have been deposited to the Cambridge Crystallographic Data Center: CCDC 1918675 (for **1**), 1,918,676 (for **2**).

2.4. Biological assays

2.4.1. Stability of pro-ligand (H_2L) and complexes *1* and *2* in biological conditions

To assess solubilities of **1** and **2** and ligand stability under the in vitro biological conditions, 50 μM solutions of pro-ligand and of **1** and **2** were incubated in Dulbecco's modified Eagle's medium (DMEM) medium for 0, 24 and 48 h at 37 °C and UV–Vis spectra were recorded in 200 to 600 nm range. All solutions were prepared from concentrated stock solutions (in DMSO) of the complexes and pro-ligand.

2.4.2. Cell culture

Human ovarian carcinoma (A2780), prostate carcinoma(PC3), colorectal carcinoma (HCT116) and breast adenocarcinoma (MCF-7) cell lines were grown in Dulbecco's modified Eagle's medium (DMEM) (Invitrogen Corp., Grand Island, NY, USA) supplemented with 10% fetal bovine serum and 1% antibiotic/antimycotic solution (Invitrogen Corp.) and maintained at 37 °C in a humidified atmosphere of 5% (*v*/v) CO_2 [41]. Normal Human fibroblasts were grown in the same conditions as A2780 cell line but DMEM medium was supplemented with 1% DMEM non-essential amino acids (Invitrogen Corp.) [42]. All cell lines were purchase from ATCC (www.atcc.org).

2.4.3. Complex exposure for dose-response curves

Cells were plated at 5000 cells/well in 96-well plates. Media were removed 24 h after platting and replaced with fresh ones containing: 0.05–75 μM of **1**, **2** or pro-ligand H_2L. All the previous solutions were prepared from concentrated stock solutions (in DMSO) of the compounds and pro-ligand.

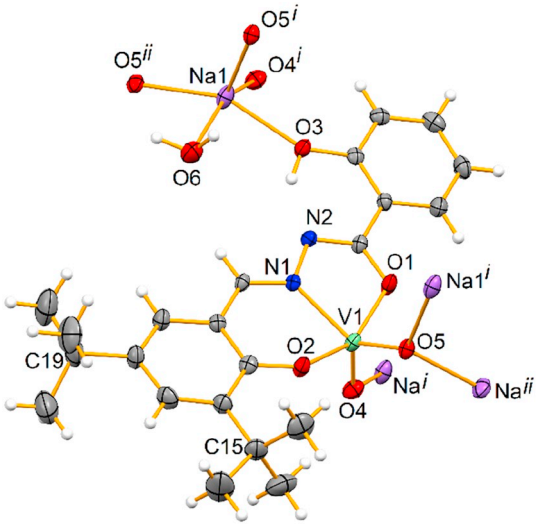

Fig. 1. Ellipsoid plot, drawn at 30% probability level, of polymer **1** with partial atom labelling schemes. Only one component of the disordered C19-containing *tert*-butyl group is represented. Symmetry codes: i) 1.5-x, −1/2-y, −z; ii) x, −y, −1/2 + z. Selected bond distances (Å) and angles (°): V1-N1 2.113(3), V1-O1 1.992(3), V1-O2 1.856(2), V1-O4 1.624(2), V1-O5 1.640(2), Na1-O3 2.336(3), Na1-O4^{i} 2.396(3), Na1-O5^{i} 2.455(3), Na1-O5^{ii} 2.370(3), Na1-O6 2.459(3), N1-N2 1.400(4), O1-V1-N1 74.00(10), O1-V1-O2 152.71(10), O1-V1-O4 97.70(12); O1-V1-O5 91.47(11); O2-V1-N1 81.92(10), O2-V1-O5 97.67(12).

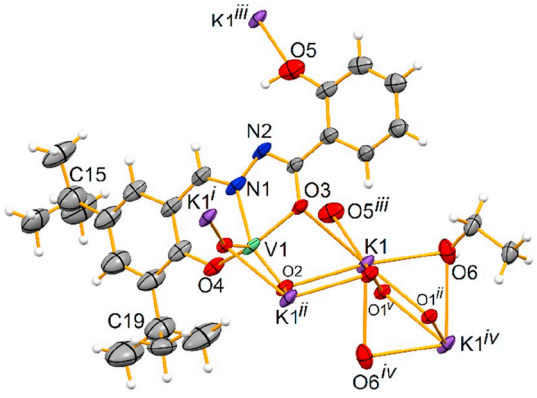

Fig. 2. Ellipsoid plot, drawn at 30% probability level, of polymer **2** bottom with partial atom labelling schemes. Only one component of the disordered O6-containing ethanol ligand is represented. Symmetry codes: i) -1 + x, y, z; ii) 1-x, −y, 1-z; iii) 1-x, 1-y, 1-z; iv) 2-x, −y, 1-z; v) 1 + x, y, z. Selected bond distances (Å) and angles (°): V1-N1 2.117(6), V1-O1 1.635(5), V1-O2 1.640(5), V1-O3 1.979(6), V1-O4 1.873(6), K1-O2 2.711(6), K1-O3 2.880(5), K1-O6 2.701(7), O1-V1-N1 102.1(2), O1-V1-O2 108.0(3), O1-V1-O3 101.9(2); O1-V1-O4 107.7(3); O2-V1-N1 148.0(3), O2-V1-O4 97.9(3).

2.4.4. Viability assays

Cells were incubated for 48 h in the presence or absence of each complex or pro-ligand, cell viability was evaluated with CellTiter 96® AQueous Non-Radioactive Cell Proliferation Assay (Promega, Madison, WI, USA), using 3-(4,5-dimethylthiazol-2-yl)-5-(3-carboxymethoxyphenyl)-2-(4-sulfophenyl)-2H-tetrazolium, inner salt (MTS) as previously described [35,41–43]. This homogeneous, colorimetric method allows determining the number of viable cells in proliferation,

cytotoxicity or chemosensitivity assays. The CellTiter 96® AQueous Assay is composed of two solutions: MTS and an electron coupling reagent (phenazinemethosulfate, PMS). MTS is bioreduced by dehydrogenase enzymes found in metabolically active cells into a formazan product that is soluble in the culture medium. The quantity of formazan product was measured in a Bio-Rad microplate reader Model 680 (Bio-Rad, Hercules, CA, USA) at 490 nm, as absorbance is directly proportional to the number of viable cells in culture.

2.4.5. Reactive oxygen species (ROS) in A2780 cells exposed to complexes 1 and 2

The induction of ROS in A2780 cells was determined by flow cytometry using the 2′,7′-dichlorodihydrofluorescein diacetate (H_2DCF-DA) dye (ThermoFisher Scientific) as described in [44,45]. This method relies on the cellular esterases to remove the acetate groups from the dye which allows for oxidation within cells with concomitant increase of fluorescence [44,45]. A2780 cells were seeded in 6-well plates and incubated for 48 h with IC_{50} concentrations of **1** and **2**. As controls, hydrogen peroxide (H_2O_2) 25 μM (positive control) and DMSO 0.1% (*v/v*) (vehicle control) were used. A2780 cells were detached with trypsin, washed with phosphate buffer solution (PBS) and incubated for 30 min with 10 μM of H_2DCF-DA at 37 °C. Cells were then analysed in an Attune acoustic focusing cytometer (ThermoFisher Scientific) and data were analysed using the respective software (Attune Cytometric Software, vs. 2.1).

2.4.6. Apoptosis induction in A2780 cells exposed to complexes 1 and 2

Apoptosis in A2780 cells was determined by flow cytometry using the Annexin V-FITC/PI (FITC: fluorescein isothiocyanate; PI: propidium iodide) dead cell apoptosis assay (Thermofisher Scientific) according to the manufacturer's instructions. Briefly, A2780 cells cultivated in 6-well plates were incubated for 48 h with IC_{50} concentrations of **1** and **2**. For controls, cells were also treated with DMSO 0.1% (solvent control) and with doxorubicin 0.4 μM (positive control). After incubation, cells were detached with trypsin, washed with PBS and incubated 15 min RT with Annexin *V*-FITC assay solution and 10 μg mL^{-1}. Cells were then analysed in an Attune acoustic focusing cytometer (ThermoFisher Scientific) and the resulting information was analysed with the respective software (Attune Cytometric Software, vs. 2.1).

2.4.7. Autophagy induction in A2780 cells exposed to complexes 1 and 2

Autophagy in A2780 cells was evaluated by flow cytometry using the Autophagy Assay Kit (Abcam) according to the manufacturer's instructions. A2780 cells were seeded in 6-well plates and incubated as described above for 48 h with IC_{50} concentrations of **1** and **2.** Cells were also treated with DMSO 0.1% (vehicle control) and with rapamycin 500 nM (positive control). Afterwards, trypsin was used to detach cells from the wells, and Assay buffer 1× was used for washing. Cells were incubated in DMEM medium with Green Stain solution and incubated for 30 min RT. Cells were collected, washed with Assay Buffer 1× and resuspended in Assay Buffer 1× before being analysed in an Attune acoustic focusing cytometer (ThermoFisher Scientific). The respective software (Attune Cytometric Software, vs. 2.1) was used to analyse the results of the experiments.

2.4.8. Statistical analysis

All data are expressed as mean ± SEM from at least three independent experiments. Statistical significance was evaluated using the Student's *t*-test; $p < 0.05$ was considered statistically significant.

3. Results and discussion

3.1. Synthesis and X-ray structural characterization

The aroylhydrazone Schiff base (3,5-di-*tert*-butyl-2-hydroxybenzylidene)-2-hydroxybenzohydrazide (H_2L) has been used to synthesize the water soluble dioxidovanadium(V) sodium (**1**) or potassium (**2**) polymer. The reaction of the aroylhydrazone (H_2L) with [VO(acac)$_2$] in refluxing ethanol (Scheme 1) results into a dark brown solution which upon addition of aqueous NaOH or KOH turns yellow at ca. pH 9. $[NaVO_2(1\kappa NOO';2\kappa O''\text{-L})(H_2O)]_n$ **(1)** and $[KVO_2(1\kappa NOO';2\kappa O';3\kappa O''\text{-L})(EtOH)]_n$ **(2)** are obtained upon slow evaporation of the corresponding yellow solution. During the course of reaction [VO(acac)$_2$] undergoes, in solution and in the presence of hydrazone Schiff base, the well-known [25–33] aerial oxidation to the oxidovanadium(V) species. Both **1** and **2** were characterized by elemental analyses, IR and NMR (^{1}H, ^{51}V) spectroscopy, ESI-MS and single crystal X-ray diffraction. In their IR spectra the characteristic symmetric and asymmetric ν(V=O) bands are observed in the region 1000 to 900 cm^{-1}, which is the signature for oxidovanadium(IV and V) compounds [25–33]. In the ESI-MS spectra, the *m/z* values indicate the presence of the dioxidovanadium(V) $\{VO_2(L)\}^-$ cores (see Experimental). The ^{1}H NMR spectra show the aromatic protons in the range δ 7.85–6.80, the benzylic protons at ca. δ 9.0 and methyl protons of the *tert*-butyl groups in the range δ 1.40–1.29. The presence of the oxidovanadium centres is observed at −538 and − 542 ppm for **1** and **2**, respectively, in the ^{51}V NMR spectrum. The X-ray crystal structures of **1** and **2** are described below.

X-ray quality crystals of **1** and **2** were obtained upon slow evaporation of their aqueous ethanolic solutions, at room temperature. The molecular structures of polymers **1** and **2** are presented in Figs. 1 and 2, respectively, with selected bond distances and angles provided in the legends. Crystal data and structure refinement details are given in Table S1 (Supplementary Material file). The asymmetric units of **1** and **2** comprise one fully deprotonated L ligand, a $\{VO_2\}^+$ assembly, the alkali metal cation and a water (in **1**) or a ethanol (in **2**) ligand. Upon symmetry expansion 2D infinite heterometallic coordination polymers are formed (Figs. S1, S2 and S3). The dianionic Schiff base ligands (L^{2-}) in both **1** and **2** coordinate to vanadium(*V*) in the enolate form, the metal exhibiting distorted (in **1**) and almost perfect (in **2**) square pyramidal NO_4 geometries (τ_5 = 0.26 or 0.05, in this order) [46]. The sodium cations in **1** display an O_5 coordination environment comprising three O_{oxido}, one $O_{phenolate}$, and one O_{water} donor atoms; in **2**, four O_{oxido}, one $O_{phenolate}$, one $O_{enolate}$, and two $O_{ethanol}$ atoms coordinate to the potassium cations. The polyhedral representations of polymers **1** and **2** (Fig. S3) indicate the former with a wide construction resulting from the one-atom contacts between the V- and the Na-polyhedrons. In polymer **2** the K-coordination polyhedrons share a face or an edge while the V-polyhedrons share two edges with the previous. In both polymers the V-polyhedrons are never connected. Probably related with these aspects and despite the difference in size of the alkali metal cation, the intramolecular V···V distances in **1** (6.601 Å) is considerably longer than that in **2** (5.604 Å), the same happening with the Na···Na (4.038 Å) relatively to the K···K one (3.785 Å). The V(V) cation is situated 0.497 (in **1**) and 0.492 Å (in **2**) away from the basal plane and towards the apical oxido ligand. The V-O_{oxido} distances in the 1.624(2) – 1.640(5) Å range (see Figs. 1 and 2 legends) are consistent with vanadium-oxygen double bonds which are commonly found in five- and six-coordinate vanadium (IV and V) complexes [25–33]. In addition, and as reported [25–33], this distance is shorter than the V-$O_{phenolate}$ [*avg.* 1.856(2) and 1.873(6) Å] and the V-$O_{enolate}$ [*avg.* 1.992(3) and 1.979(6) Å] lengths. Therefore, and on the whole, the alkali metals in **1** and **2** are directly engaged with only one L^{-2} moiety. The Na−O bond distances (in **1**) range from 2.336(3) to 2.459(3) Å and the K−O ones (in **2**) range from 2.701(7) to 3.052(8) Å.

3.2. Biological assays

3.2.1. Stability in biological media

Before performing the biological assays, it is important to assess the stability of both the ligand and complexes in a more complex water-based medium. In this regard, solutions of 50 μM of ligand and of both

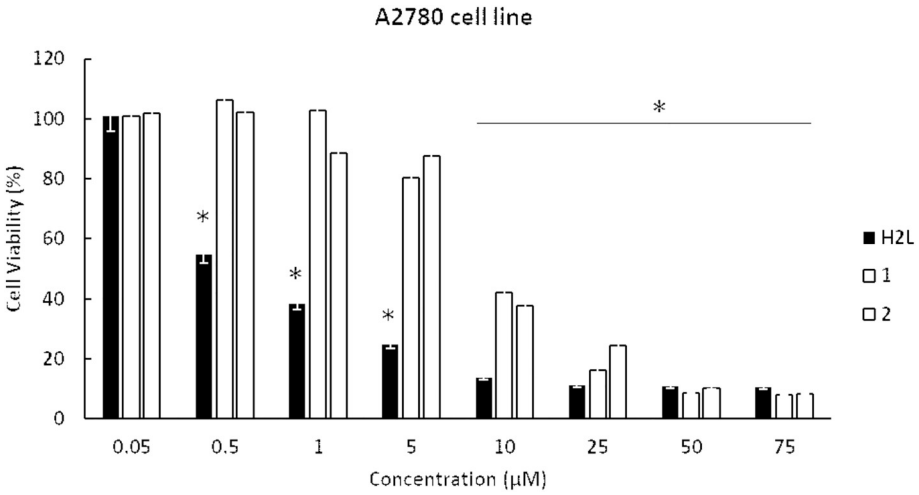

Fig. 3. Cell Viability (%) of pro-ligand **H_2L** (black bar) and polymers **1** (white bar) and **2** (grey bar) in A2780 cancer cell line and evaluated after 48 h of exposure to increasing concentrations of each ligand or complex. Cell viability percentage was determined by the MTS method. DMSO 0.1% (*v*/v) was used as vehicle control condition. The results presented are average ± SD of three independent assays. The symbol * indicates a *p*-value < 0.05.

compounds were prepared in DMEM medium (from stock solutions in DMSO) and incubated at 37 °C for 24 h and 48 h. Spectra were recorded at time 0 h, 24 h and 48 h. Supplementary Fig. S4 shows that only minute spectral changes were observed, which indicates a very good stability over time, with **1** showing peaks with the same pattern and intensity from 0 to 48 h. Concerning the pro-ligand, a very slight decrease in absorbance at 360 nm is observed after 48 h of incubation in DMEM (Supplementary Fig. S4). Considering these results, we next analysed the effect of **1** and **2** in cancer and normal cells viability.

3.2.2. Cell viability

Concentration-response curves for the vanadium polymers **1** and **2** were obtained in A2780, PC3, HCT116 and MCF-7 cancer cell lines (Fig. 3 and Supplementary Fig. S5). These concentration-response curves were used to assess the relative IC_{50} (concentration that reduces cell proliferation by 50% as compared to control) (Table 1 and Table S2). The antiproliferative effect of polymers **1** and **2** in the cancer cell lines tested followed the trend A2780 > HCT116 > PC3 > MCF-7, with a stronger effect induced by polymer **1** compared to **2** in all cancer cell lines (Table 1, Fig. 3 and Supplementary Table S2 and Fig. S5). Considering this higher antiproliferative effect in ovarian carcinoma cells (A2780) for both polymers, we then tested the antiproliferative effect of the pro-ligand **H_2L** in this cell line (Fig. 3). A very high antiproliferative effect was observed for **H_2L** following the trend **H_2L** > **1** > **2**, meaning that coordination of **H_2L** with vanadium attenuates the high cytotoxic activity of the pro-ligand in A2780 cells (Fig. 3 and Table 1).

Because several metal complexes induce a high cytotoxicity in normal cells (e.g., side effects associated with cisplatin treatment), the cellular effect of **H_2L**, **1** and **2** in normal human fibroblasts was assessed. It was possible to observe that **H_2L** induces a high loss of normal cell viability compared to **1** and **2** (Table 1). Indeed, for concentrations up to 75 μM of **1** or **2** no reduction of normal cell viability was observed (Table 1), while the IC_{50} value for **H_2L** in fibroblasts is even lower than the IC_{50} of cisplatin in HCT116 carcinoma cell line (15.2 μM) [10]. Comparing these results with other dioxidovanadium(V) polymers that used aroylhydrazone ligands [10], it is possible to observe that the polymers **1** and **2** presented in this work are more effective in the MCF-7 cell line than those already described in [10] (Supplementary Table S3). In the HCT116 cell line, polymer **1** (this work) and complex **1** (from [10]) are more cytotoxic than polymer **2** (this work) and complex **2** (from [10]). In the present work and in [10], the metal source is the same, $VO(aca)_2$, which presents IC_{50} values above 50 μM in HCT116 and MCF-7 cell lines [10]. Thus, the differences in polymer cytotoxicity are due to the **H_2L** used in this work (Fig. 3 and Table 1) which presents higher toxicity than the ligands used in [10]. Despite coordination of **H_2L** with vanadium produces polymers with lower cytotoxicity in cancer cell lines, it also significantly decreases cytotoxicity to normal fibroblast cells that is extremely important in the context of cancer therapy. Interestingly, the IC_{50} (assessed in the same experimental conditions) for polymers **1** and **2** in A2780 cells are in the same range of that of cisplatin (3.4 ± 0.2 μM) [47]. Comparing the cytotoxicity of our polymers with other vanadium(IV) and vanadium(V) complexes, and despite the huge variability in cell lines and methodologies used to determine IC_{50} values (Supplementary Table S3), it is possible to observe that our values are in the same order of magnitude than those already described for MCF-7. It is interesting to note that this cytotoxicity is highly dependent on the ligand, with complexes bearing 1,10-phenantroline showing a high cytotoxicity particularly in human hepatocellular carcinoma (HepG2), mouse myeloma cells (Ag8.653), human glioblastoma cells (U251) and B cell precursor leukemia cell (NALM6) (Supplementary Table S3). These results (high cytotoxicity of 1,10-phenantroline complexes) are also in agreement with previous results from our group [48–50].

Taken together, these results highlight the potential of the alkali metal-vanadium polymers **1** and **2** for further biological studies.

Vanadium(V) complexes have been described to exert biological activity through generation of reactive oxygen species, ROS, and the permeabilization of cell membranes, [51,52]. Therefore, we investigated if these compounds were capable to induce the accumulation of ROS in A2780 cells (Fig. 4).

The exposure of A2780 cells to **1** and **2** induces an increase of 2.45× and 1.95×, respectively, in the amount of intracellular ROS when compared to DMSO control (Fig. 4). Interestingly, both compounds induce ROS at a similar level compared to the positive control (H_2O_2) (Fig. 4). These results agree with previous data that vanadium complexes trigger oxidative stress [53,54]. Since ROS have been described as a trigger for apoptosis, the induction of apoptosis (Fig. 5) in A2780 cells was also investigated [55].

Results show that the exposure of A2780 cells to **1** and **2** for 48 h induce apoptosis in 2.5% and 3.5%, respectively. Normalizing to the values of the DMSO control (0.83%), this corresponds to an increase of 6.7× and 9.6× in apoptotic cells (Fig. 5). No significant variation on

Table 1
Values of relative IC_{50} (μM) of pro-ligand **H_2L** and polymers **1** and **2** in A2780 cancer cell line and in normal human primary fibroblasts.

IC_{50} (μM)	A2780	Fibroblasts
H_2L	0.8 ± 0.05	10 ± 0.2
1	8.2 ± 0.1	> 50
2	11.3 ± 0.2	> 50

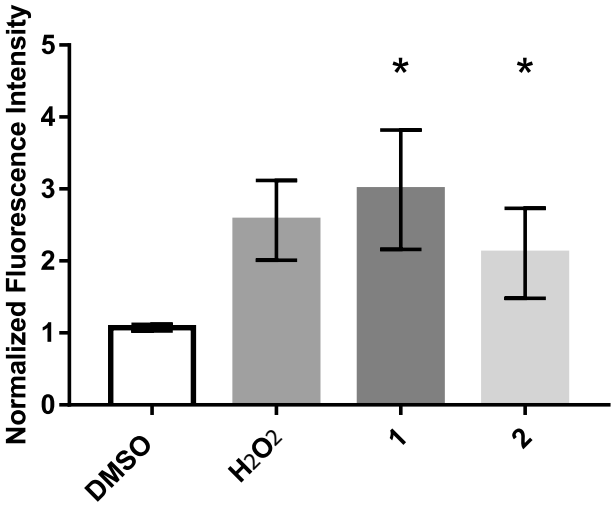

Fig. 4. Reactive oxygen species (ROS) induced in A2780 cells by 48 h exposure to IC_{50} concentrations of **1** and **2** evaluated by flow cytometry. DMSO 0.1% was the solvent control and, as a positive control, H_2O_2 25 μM was used. (* *p*-value < 0.05).

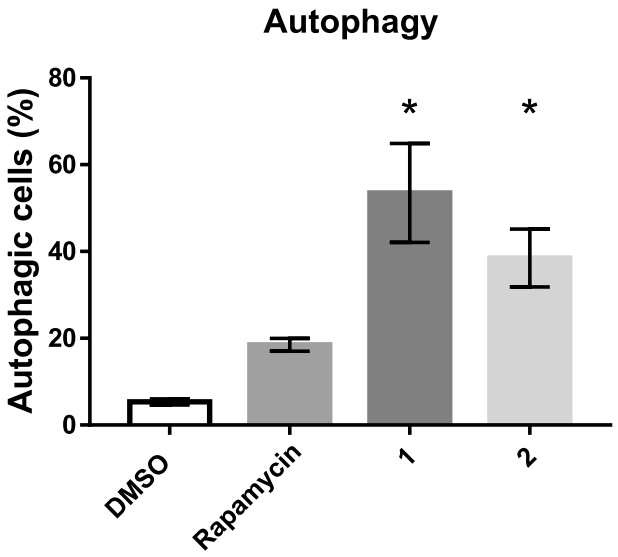

Fig. 6. Induction of autophagy in A2780 cells after 48 h exposure to IC_{50} concentrations of complexes **1** and **2** evaluated by flow cytometry. DMSO 0.1% (*v*/v) was the solvent control and Rapamycin (500 nM) was used as positive control. (* *p*-value < 0.05).

necrotic cells was observed when compared to both negative control and doxorubicin (Fig. 5). This is a positive feature since necrosis is associated with the recruitment of immune and inflammatory cells which exert tumor promoting activity by inducing angiogenesis, proliferation and invasion [56].

Despite the induction of apoptosis, the levels obtained by exposure of cells to the IC_{50} concentrations of **1** and **2** are low compared to the IC_{50} concentration of doxorubicin (Fig. 5). This mean that cells might also be triggering also other cell death pathways as previously observed [54]. In this regard the induction of autophagy in A2780 cells after 48 h exposure to IC_{50} concentrations of **1** and **2** was also assessed (Fig. 6).

It is possible to observe that 53.5% of A2780 cells exposed to **1** were autophagic and 38.5% of A2782 cells exposed to **2** displayed autophagic labelling (Fig. 6). This corresponds to an increase of 10× and 7.2× of autophagic cells regarding the DMSO control (Fig. 6). Surprisingly, the levels of autophagy induced by the complexes are higher than the one observed for the positive control Rapamycin (Fig. 6).

Taken together our results show that both complexes induce ovarian carcinoma cell death via apoptosis and autophagy, but autophagy is the main biological cause of the reduction of cell viability (Figs. 3, 5 and 6) and that ROS may play an important role in triggering cell death (Fig. 4). In a previous report, dioxidovanadium polymers with similar aroylhydrazone ligands also reduced HCT116 cell viability mainly by apoptosis, rather than autophagy [10].

4. Conclusions

We have successfully synthesized and characterized the water soluble heterometallic sodium or potassium-dioxidovanadium polymers, $[NaVO_2(1\kappa NOO';2\kappa O''\text{-L})(H_2O)]_n$ **(1)** and $[KVO_2(1\kappa NOO';2\kappa O';3\kappa O''\text{-L})(EtOH)]_n$ **(2)**. The compounds show a good stability in biological medium for 48 h. Despite the very similar effect of both in ovarian carcinoma cell line viability, polymer **1** showed the highest effect in the reduction of this cancer cell viability with an IC_{50} of 8.2 μM (in the same range as cisplatin - IC_{50} of 3.4 μM; obtained in the same experimental conditions). Interestingly, in contrast to the precursor molecule, both polymers had no effect in healthy human fibroblasts growth for concentrations up to 75 μM. Furthermore, our results show that autophagy is the main cause of the viability reduction observed in A2780 cells exposed to **1** and **2**. Nevertheless, cell death via apoptosis is also observed. Both cell death events are probably triggered by the generation of ROS caused by **1** and **2**. Taken together these results demonstrate the potential of both alkali metal-vanadium polymers for further in vivo assays.

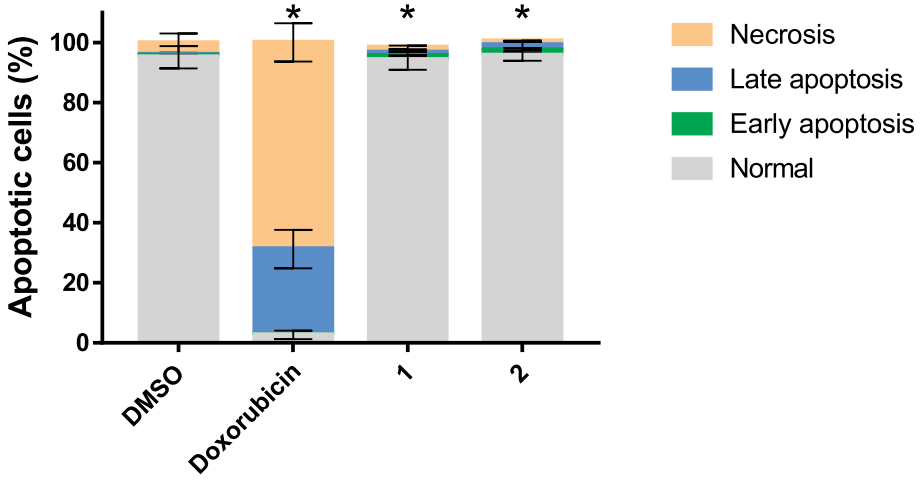

Fig. 5. Induction of apoptosis in A2780 cells after 48 h exposure to IC_{50} concentrations of **1** and **2** evaluated by flow cytometry. DMSO 0.1% (*v*/v) was the solvent control and doxorubicin (IC_{50} 0.4 μM) was used as positive control. (* p-value < 0.05 for early and late apoptosis for all samples and in the doxorubicin sample also for necrosis).

Acknowledgment

The authors gratefully acknowledge the Fundação para a Ciência e a Tecnologia (FCT), Portugal, and its projects PTDC/QEQ-ERQ/1648/2014 and UID/QUI/00100/2019. M.S. acknowledges the FCT and IST for a working contract "DL/57/2017" (Contract no. IST-ID/102/2018). This work was also supported by the Applied Molecular Biosciences Unit - UCIBIO which is financed by national funds from FCT/MCTES (UID/Multi/04378/2019). Authors are thankful to the Portuguese NMR Network (IST-UL Centre) for access to the NMR facility and the IST Node of the Portuguese Network of mass-spectrometry for the ESI-MS measurements.

Appendix A. Supplementary data

Table S1 and Figs. S1-S3. CCDC 1918675 (for **1**) and 1918676 (for **2**) contain the supplementary crystallographic data for this paper. This data can be obtained free of charge from The Cambridge Crystallographic Data Centre via www.ccdc.cam.ac.uk/data_request/cif. Supplementary data to this article can be found online at doi:https://doi.org/10.1016/j.jinorgbio.2019.110811

References

[1] K. Kustin, J. Costa Pessoa, D.C. Crans (Eds.), Vanadium: The Versatile Metal, ACS Symposium Series, 974 Oxford University Press, American Chemical Society, Washington, DC, 2007.
[2] D. Rehder, Dalton Trans. 42 (2013) 11749–11761.
[3] D. Rehder, Future Med. Chem. 4 (2012) 1823–1837.
[4] P. Noblía, E.J. Baran, L. Otero, P. Draper, H. Cerecetto, M. González, O.E. Piro, E.E. Castellano, T. Inohara, Y. Adachi, H. Sakurai, D. Gambino, Eur. J. Inorg. Chem. (2004) 322–328.
[5] A. Messerschmidt, R. Wever, Proc. Natl. Acad. Sci. U. S. A. 93 (1996) 392–399.
[6] D.C. Crans, K.A. Woll, K. Prusinskas, M.D. Johnson, E. Norkus, Inorg. Chem. 52 (2013) 12262–12275.
[7] G.R. Willskya, L.-H. Chi, M. Godzala III, P.J. Kostyniak, J.J. Smeed, A.M. Trujillo, J.A. Alfano, W. Ding, Z. Hu, D.C. Crans, Coord. Chem. Rev. 255 (2011) 2258–2269.
[8] J.C. Pessoa, S. Etcheverry, D. Gambino, Coord. Chem. Rev. 301 (2014) 24–48.
[9] D. Rehder, Bioinorganic Vanadium Chemistry, Wiley, Chichester, U. K., 2008.
[10] M. Sutradhar, A.R. Fernandes, J. Silva, K.T. Mahmudov, M.F.C. Guedes da Silva, A.J.L. Pombeiro, J. Inorg. Biochem. 155 (2016) 17–25.
[11] M. Sutradhar, T. Roy Barman, G. Mukherjee, M. Kar, S.S. Saha, M.G.B. Drew, S. Ghosh, Inorg. Chim. Acta 368 (2011) 13–20.
[12] E. Kioseoglou, S. Petanidis, C. Gabriel, A. Salifoglou, Coord. Chem. Rev. 301-302 (2015) 87–105.
[13] D.C. Crans, A.S. Tracey, ACS Symp. Ser. 711 (1998) 2–29.
[14] K.H. Thompson, C. Orvig, Coord. Chem. Rev. 219 (2001) 1033–1053.
[15] A.M. Evangelou, Crit. Rev. Oncol. Hematol. 42 (2002) 249–265.
[16] R.S. Ray, B. Ghosh, A. Rana, M. Chatterjee, Int. J. Cancer 120 (2006) 13–23.
[17] Y. Dong, R.K. Narla, E. Sudbeck, F.M. Uckun, J. Inorg. Biochem. 78 (2000) 321–330.
[18] S.B. Etcheverry, E.G. Ferrer, L. Naso, J. Rivadeneira, V. Salinas, P.A.M. Williams, J. Biol. Inorg. Chem. 13 (2008) 435–447.
[19] N. Domingues, J. Pelletier, C.-G. Ostenson, M.M.C.A. Castro, J. Inorg. Biochem. 131 (2014) 115–122.
[20] L. Novotny, S.B. Kombian, J. Cancer Res Updates. 3 (2014) 97–102.
[21] I. Correia, S. Roy, C.P. Matos, S. Borovic, N. Butenko, I. Cavaco, F. Marques, J. Lorenzo, A. Rodríguez, V. Moreno, J.C. Pessoa, J. Inorg. Biochem. 147 (2015) 134–146.
[22] I. Correia, P. Adão, S. Roy, M. Wahba, C. Matos, M.R. Maurya, F. Marques, F.R. Pavan, C.Q. Leite, F. Avecilla, J.C. Pessoa, J. Inorg. Biochem. 141 (2014) 83–93.
[23] Z. Chi, L. Zhu, X. Lu, H. Yu, Bing Liu, Z. Anorg. Allg. Chem. 638 (2012) 1523–1530.
[24] A. Bishayee, A. Waghray, M.A. Patel, M. Chatterjee, Cancer Lett. 294 (2010) 1–12.
[25] M. Sutradhar, A.J.L. Pombeiro, Cord. Chem. Rev. 265 (2014) 89–124.
[26] M. Sutradhar, L.M.D.R.S. Martins, M.F.C. Guedes da Silva, A.J.L. Pombeiro, Coord. Chem. Rev. 301–302 (2015) 200–239.
[27] M. Sutradhar, G. Mukherjee, M.G.B. Drew, S. Ghosh, Inorg. Chem. 46 (2007) 5069–5075.
[28] M. Sutradhar, N.V. Shvydkiy, M.F.C. Guedes da Silva, M.V. Kirillova, Y.N. Kozlov, A.J.L. Pombeiro, G.B. Shul'pin, Dalton Trans. 42 (2013) 11791–11803.
[29] M. Sutradhar, M.V. Kirillova, M.F.C. Guedes da Silva, L.M.D.R.S. Martins, A.J.L. Pombeiro, Inorg. Chem. 51 (2012) 11229–11231.
[30] M. Sutradhar, G. Mukherjee, M.G.B. Drew, S. Ghosh, Inorg. Chem. 45 (2006) 5150–5161.
[31] M. Sutradhar, L.M.D.R.S. Martins, M.F.C. Guedes da Silva, A.J.L. Pombeiro, Appl. Catal. A Gen. 493 (2015) 50–57.
[32] M. Sutradhar, T. Roy Barman, S. Ghosh, M.G.B. Drew, J. Mol. Struct. 1020 (2012) 148–152.
[33] M. Sutradhar, L.M.D.R.S. Martins, S.A.C. Carabineiro, M.F.C. Guedes da Silva, J.G. Buijnsters, J.L. Figueiredo, A.J.L. Pombeiro, ChemCatChem 8 (2016) 2254–2266.
[34] M. Sutradhar, T. Roy Barman Rajeshwari, A.R. Fernandes, F. Paradinha, C. Roma-Rodrigues, M.F.C. Guedes da Silva, A.J.L. Pombeiro, J. Inorg. Biochem. 175 (2017) 267–275.
[35] Y. Li, Z. Yang, M. Zhou, Y. Li, J. He, X. Wang, Z. Lin, RSC Adv. 7 (2017) 41527–41539.
[36] G.H. Chimmalagi, U. Kendur, S.M. Patil, K.B. Gudas, C.S. Frampton, M.B. Budri, C.V. Mangannavar, I.S. Muchchand, Appl. Organomet. Chem. 32 (2018) e4337.
[37] M. Sutradhar, L.M.D.R.S. Martins, M.F.C. Guedes da Silva, C.-M. Liu, A.J.L. Pombeiro, Eur. J. Inorg. Chem. (2015) 3959–3969.
[38] Bruker, APEX2, Bruker AXS Inc., Madison, Wisconsin, USA, 2012.
[39] Crystal structure refinement with SHELXL, G. M. Sheldrick, Acta Cryst, 2015 C71, 3–8, https://doi.org/10.1107/S2053229614024218.
[40] L.J. Farrugia, J. Appl. Crystallogr. 45 (2012) 849–854.
[41] O.A. Lenis-Rojas, M.P. Robalo, A.I. Tomaz, A. Carvalho, A.R. Fernandes, F. Marques, M. Folgueira, J. Yáñez, D. Vázquez-García, M.L. Torres, A. Fernández, J.J. Fernández, Inorg. Chem. 57 (2018) 13150–13166.
[42] R. Mendes, P. Pedrosa, J.C. Lima, A.R. Fernandes, P.V. Baptista, Sci. Rep. 7 (2017) 10872.
[43] T.F. Silva, L.M. Martins, M.F.C. Guedes da Silva, M.L. Kuznetsov, A.R. Fernandes, A. Silva, C.J. Pan, J.F. Lee, B.J. Hwang, A.J.L. Pombeiro, Chem. Asian J. 9 (2014) 1132–1143.
[44] A. Maron, K. Czerwinska, B. Machura, L. Raposo, C. Roma-Rodrigues, A.R. Fernandes, J.G. Malecki, A. Szlapa-Kula, S. Kula, S. Krompiec, Dalton Trans. 47 (2018) 6444–6463.
[45] K. Das, A. Datta, C. Massera, C. Roma-Rodrigues, M. Barroso, P.V. Baptista, A.R. Fernandes, J. Coord. Chem. 72 (2019) 920–940.
[46] A.W. Addison, T.N. Rao, J. Reedijk, J. van Rijn, G.C. Verschoor, J. Chem. Soc. Dalton Trans. (1984) 1349–1356.
[47] K. Czerwińska, B. Machura, S. Kula, S. Krompiec, K. Erfurt, C. Roma-Rodrigues, A.R. Fernandes, L.S. Shul'pina, N.S. Ikonnikov, G.B. Shul'pin, Dalton Trans. 46 (2017) 9591–9604.
[48] A.R. Fernandes, J. Jesus, P. Martins, S. Figueiredo, D. Rosa, L.M.R.D.R.S. Martins, M.L. Corvo, M.C. Carvalheiro, P.M. Costa, P.V. Baptista, J. Control. Release 245 (2017) 52–61.
[49] D.V. Luís, J. Silva, A.I. Tomaz, R.F.M. de Almeida, M. Larguinho, P.V. Baptista, L.M.D.R.S. Martins, T.F.S. Silva, P.M. Borralho, C.M.P. Rodrigues, A.S. Rodrigues, A.J.L. Pombeiro, A.R. Fernandes, J. Biol. Inorg. Chem. 19 (2014) 787–803.
[50] T.F.S. Silva, P. Smoleński, L.M.D.R.S. Martins, M.F. Guedes da Silva, A.R. Fernandes, D. Luis, A. Silva, S. Santos, P.M. Borralho, C.M.P. Rodrigues, A.J.L. Pombeiro, Eur. J. Inorg. Chem. 21 (2013) 3651–3658.
[51] M.J. Hosseini, F. Shaki, M. Ghazi-Khansari, J. Pourahmad, Metallomics 5 (2013) 152–166.
[52] L.A. Soriano-Agueda, C. Ortega-Moo, J. Garza, J.A. Guevara-García, R. Vargas, Comput. Theor. Chem. 1077 (2016) 99–105.
[53] Y. Zhao, L. Ye, H. Liu, Q. Xia, Y. Zhang, X. Yang, K. Wang, J. Inorg. Biochem. 104 (2010) 371–378.
[54] S. Kowalski, S. Hać, D. Wyrzykowski, A. Zauszkiewicz-Pawlak, I. Inkielewicz-Stępniak, Oncotarget 8 (2017) 60324–60341.
[55] O. Kepp, L. Galluzzi, M. Lipinski, J. Yuan, G. Kroemer, Nat. Rev. Drug Discov. 10 (2011) 221–237.
[56] S.Y. Lee, M.K. Ju, H.M. Jeon, E.K. Jeong, Y.J. Lee, C.H. Kim, H.G. Park, S.I. Han, H. S. Kang, Oxidative Med. Cell. Longev. (2018) Article ID 3537471.